To appear in ApJ
Preprint typeset using LaTeX style emulateapj v. 11/10/09

arXiv:1106.1180v1 [astro-ph.CO] 6 Jun 2011

A SYSTEMATIC SEARCH FOR MASSIVE BLACK HOLE BINARIES IN SDSS SPECTROSCOPIC SAMPLE

P. Tsalmantza[1], R. Decarli[1], M. Dotti[2,3], David W. Hogg[1,4]

To appear in ApJ

ABSTRACT

We present the results of a systematic search for massive black hole binaries in the Sloan Digital Sky Survey spectroscopic database. We focus on bound binaries, under the assumption that one of the black holes is active. In this framework, the broad lines associated to the accreting black hole are expected to show systematic velocity shifts with respect to the narrow lines, which trace the rest-frame of the galaxy. For a sample of 54 586 quasars and 3 929 galaxies at redshifts $0.1 < z < 1.5$ we brute-force model each spectrum as a mixture of two quasars at two different redshifts. The spectral model is a data-driven dimensionality reduction of the SDSS quasar spectra based on a matrix factorization. We identified 32 objects with peculiar spectra. Nine of them can be interpreted as black hole binaries. This doubles the number of known black hole binary candidates. We also report on the discovery of a new class of extreme double-peaked emitters with exceptionally broad and faint Balmer lines. For all the interesting sources, we present detailed analysis of the spectra, and discuss possible interpretations.

Subject headings: methods: data analysis; methods: statisticals; quasars: general; quasars: emission lines

1. INTRODUCTION

Massive black hole (BH) pairs are the natural outcome of mergers through the hierarchical formation of galaxies. Examples of unbound BH pairs, with separations of $\lesssim 1$ kpc, have been observed, as in the prototypical case of NGC 6240 (Komossa et al. 2003, see Colpi & Dotti 2009 for a recent review). At separations of $\sim$ few pc the two BHs start experiencing their own gravitational interaction, binding in a BH binary (BHB). Observing BHBs is challenging, since they cannot be spatially resolved in optical and X-ray. The only spatially resolved BHB candidate to date is hosted by the elliptical galaxy 0402+379 (Maness et al. 2004; Rodriguez et al. 2006). The two flat-spectrum radio sources, corresponding to the two components of the candidate BHB, have a projected separation of ≈ 7 pc. At the distance of 0402+379 ($z = 0.055$) this corresponds to few milliarcsec, an angular scale that can be probed only through radio interferometry. A second BHB candidate is the BL Lac OJ287 (see Valtonen et al. 2008, and references therein). It shows a ≈ 12 yr modulation in its light curve, that has been interpreted as related to the orbital period of a BHB lurking in the nucleus of the AGN.

All the other BHB candidates discussed to date have been identified by studying their optical and near–infrared spectra. In a BHB scenario, the broad lines (BLs) emitted by gas bound to each BH may be red- or blue-shifted with respect to their host galaxy redshift, as a consequence of the Keplerian motion of the binary (Begelman, Blandford & Rees 1980). Furthermore, the BL region of each BH can be perturbed and stripped by the gravitational potential of the companion, resulting in peculiar flux ratios between BLs with different ionization potential (Montuori et al. 2010). This spectroscopic approach does not suffer any angular resolution limitations: Actually, the closer (and more massive) the binary is, the more shifted/deformed the BLs are. Thanks to the existence of large spectroscopic surveys, such as the Sloan Digital Sky Survey (SDSS), a large region of the sky can be probed. Up to date five spectroscopically identified candidates have been presented: J0927+2943 (Komossa, Zhou & Lu 2008; Bogdanovic, Eracleous & Sigurdsson 2009; Dotti et al. 2009), J1536+0441 (Boroson & Lauer 2009), J1050+3456 (Shields et al. 2009), 4C+22.25 (J1000+2233 in this paper, Decarli et al. 2010b), and J0932+0318 (Barrows et al. 2011). Such a small number of objects is marginally compatible with the theoretically predicted number of sub-parsec BHBs at $z \lesssim 0.7$ (5–10, given the merger rate and under reasonable assumptions on the binary lifetime and observability; see Volonteri et al. 2009).

The spectroscopic approach has an obvious drawback: a peculiar spectrum does not guarantee the presence of a BHB in the nucleus of the host. As an example, an unobscured BHB with both BHs active could resamble the spectrum of a double peaked emitter (see, e.g., Eracleous & Halpern 1994), where broad double–peaked lines are emitted because of the almost edge–on, disk–like structure of the BL region of a single BH. A binary with a single accreting BH would show a single shifted BL. If the shift corresponds to a relatively small velocity along the line of sight ($\lesssim 4\,000$ km s^{-1}), the same signature could be emitted by a remnant of a binary coalescence, recoiling because of anisotropic gravitational wave emission (e.g. Komossa, Zhou & Lu 2008)[5]. Fi-

---

[1] Max-Planck Institut für Astronomie, Königstuhl 17, D-69117, Heidelberg, Germany. E-mail: vivitsal@mpia.de, decarli@mpia.de
[2] Max-Planck-Institut für Astrophysik, Karl-Schwarzschild-Str. 1, D-85748, Garching, Germany.
[3] Dipartimento di Fisica G. Occhialini, Università degli Studi di Milano Bicocca, Piazza della Scienza 3, 20126 Milano, Italy
[4] Center for Cosmology and Particle Physics, Department of Physics, New York University, 4 Washington Place, New York, NY 10003, USA

[5] If the galaxy merger is gas rich, the maximum recoil velocity is expected to be $\lesssim 100$ km s^{-1} (Bogdanovic, Reynolds & Miller 2007; Dotti et al. 2010; Volonteri et al. 2010; Kesden et al. 2010).

nally, both the cases can be reproduced by a chance superposition of two AGN (or an AGN-galaxy superposition) within the angular resolution of the used spectrograph (e.g. Heckman et al. 2009). The simplest way to discriminate between these scenarios and the BHB hypothesis would be to look for a periodic oscillation of the BL shifts around the host galaxy redshift. However, the orbital period of the binary could be too long to be easily observed (Begelman, Blandford & Rees 1980). For these reasons other possible explanations have been proposed for all the BHB candidates discussed in literature.

To overcome the paucity of BHB candidates and the uncertainties related to their interpretation, we depict two ways:
Theoretically a better description of the spectrum of BHB is needed, in order to identify other characteristic signatures of binaries. Few attempt as been made up to date (see, e.g. Bogdanovic et al. 2008; Bogdanovic, Eracleous & Sigurdsson 2009; Shen & Loeb 2010; Montuori et al. 2010).
Observationally all the BHB candidates lurking in large spectroscopic catalogue must be identified, through a meticulous study of all the possible spectra, in order to allow for follow-up studies on a significant sample of objects.

In this paper we explore the second path, describing the results we obtained from a comprehensive search of BHBs in the SDSS DR7. The code we use, described in Section 2, automatically detects sources with a spectrum consistent with a BHB, a double peaked emitter, a superposition, or a recoiling BH. We present all the peculiar objects we find in Section 3, where, for each object, we compare our results with previous findings available in the literature. Conclusions are drawn in Section 4. Throughout the paper we will assume a standard cosmology with $H_0 = 70$ km s^{-1} Mpc^{-1}, $\Omega_{\rm m} = 0.3$ and $\Omega_\Lambda = 0.7$.

2. THE METHOD

2.1. *Present analysis*

In this study we perform an automatic and systematic search for BHB candidates in SDSS catalogue, looking for composite spectra of two sources with a velocity difference up to 30 000 km s^{-1}. More specifically, we look for the presence of two sets of emission lines (one broad and one narrow) with a small separation between them, caused by the Keplerian rotation of one component of the binary system. For this purpose we use the method described in Tsalmantza & Hogg (2011). As a first step we extract a small set of components that can sufficiently reconstruct the SDSS QSO spectra by using HMF (Heteroscedastic Matrix Factorization or HMF), a bilinear model optimized with probabilistically justified weighted least-squares objective function, analogous to principal components analysis but making use of the observational noise model. The method uses a subset of data at rest-frame wavelengths, described in detail in Section (2.2), as a training set to define the set of basis functions that minimize the scalar χ^2_ϵ:

$$\chi^2_\epsilon \equiv \sum_{i=1}^{N}\sum_{j=1}^{M}\frac{\left[f_{ij}-\sum_{k=1}^{K}a_{ik}\,g_{kj}\right]^2}{\sigma^2_{ij}} + \epsilon\sum_{k=1}^{K}\sum_{\ell=2}^{M}\left[g_{k\ell}-g_{k(\ell-1)}\right]^2 \quad , \tag{1}$$

where the first term corresponds to the total χ^2 of the fit of the training data points f_{ij} with errors σ_{ij}, by a set of K components g_{kj} and coefficients a_{ik}, over all the N spectra and the M pixels of the training set. The second term corresponds to a smoothing prior or regularization that prefers small pixel-to-pixel variations in each resulting component. The strength of the smoothing is set by the scalar ϵ. An iterative procedure is used to minimize χ^2_ϵ. In each step, we fix g_{kj} and estimate the optimal a_{ik}, and then hold the a_{ik} fixed and estimate the optimal g_{kj}. The procedure is repeated until the solution converges. We initialize the fitting with the output of PCA when applied to an extended set of training spectra.

We then use the resulting set of components to fit each observed spectrum at the redshift provided by SDSS. After that, we repeat the fitting using *two* sets of components at different redshifts. Here one set is assumed to be at the SDSS redshift, while the second is free to vary over a broad range of z, corresponding to velocity differences up to 30 000 km s^{-1}. If a second redshift system is present, we expect the fit to significantly improve when we add the second set of components. This procedure has already been proven to successfully identify four of the known BHB candidates (J0927+2943, J1536+0441, J1050+3456, and J1000+2233, see Tsalmantza & Hogg 2011) with an estimate of the velocity shifts between the two sets of lines consistent with what obtained in previous studies.

2.2. *The training sample*

To train the HMF we use the same training set of quasar spectra that was used in Tsalmantza & Hogg (2011). The sample consists of spectra in the redshift range 0.1-1.5. However, since we are mainly interested in detecting shifts between the narrow and the broad emission lines in the QSO spectra, we check if our method is more sensitive in detecting interesting objects when one of the two sets of components used to fit each spectrum is representative of spectra with only narrow emission lines. To define components that include only narrow lines, we use galaxy spectra for the training of the HMF. The galaxy sample consists of spectra classified spectroscopically as galaxies in SDSS with S/N>20 and EW of the [O II] and [O III] lines larger than 20 (10 856 spectra).

All spectra used for the training and the application of the method are derived from the 7th Data Release (DR7) of SDSS. Pixels with any of the flags: SP_MASK_FULLREJECT, SP_MASK_BRIGHTSKY, SP_MASK_NODATA, SP_MASK_NOSKY or pixels that correspond to zero noise were treated as masked. All the spectra and their noise were moved to the rest-frame (assuming $z = z_{\rm SDSS}$), resulting in spectra with different spectral coverage. However, both HMF and PCA (the output of which was used as an initialization to the HMF) require common wavelengths for all the training

---

In this case, a significant shift between the different sets of lines would not be compatible with a recoiling BH.

spectra. The common wavelength range was defined by the pixels that included information for at least 10 spectra of each type (i.e. galaxies or QSOs). The final wavelength coverage was 1522.299-8352.183 Å for the QSOs and 3044.388-9193.905 Å for the galaxies, corresponding to 7394 and 4801 pixels respectively. As a last step before the application of the method all spectra were interpolated to common wavelengths selected for each type of source using cubic splines. The selected wavelengths are uniformly distributed in log space as in the case of the original SDSS wavelengths. For the resulting spectra we interpolated linearly the values of the masked pixels.

PCA was performed separately for the QSO and the galaxy sample, using a number of spectra equal to the number of pixels selected for each source. The training spectra were first projected into a subspace orthogonal to the mean spectrum of the data set and the flux in each spectral bin was divided with the RMS of the noise in that bin, for all the non-masked pixels in the training sample. The PCA results were used as an initialization to the HMF. The method was run for a subset of approximately 1 000 spectra of each type for a different number of components and for 16 iterations, until convergency. This test was also performed for four different values (1,3,10 and 30) of the smoothing scalar ϵ. To perform a simple cross validation, the resulting components were also used to fit another subset of 1 000 test spectra for each type. Based on these tests, we decided to use 14 and 7 components for the QSOs and galaxies and ϵ values of 10 and 1 respectively. Those numbers were also defined by using the spectra of the known BHB candidates and testing the ability of the components to detect them.

2.3. *Selection criteria*

We apply our newly developed fitting scheme to all the 54 586 QSO spectra of SDSS in the redshift range 0.1-1.5. Additionally, since one of the known BHB candidates (4C+22.25, Decarli et al. 2010b) is classified spectroscopically as a galaxy in the SDSS catalog, we also applied the method to objects with redshift from 0.2-1.5, that are classified by SDSS as galaxies and have fiber magnitudes that correspond to $u - g < 0.8$, $g - r < 1.5$, $r - i < 1.0$ and $g < 21$. We note that the majority of these sources (3 518 out of 3 929) were targeted as quasar candidates by SDSS. For each spectrum the fitting was performed for all the combinations of the extracted QSO and galaxy components: i) two QSO components for both the spectral components (hereafter QSO-QSO), ii) a QSO component for the spectrum at the SDSS redshift and a galaxy components at the second redshift (QSO-Galaxy) and iii) the opposite of case (ii) (Galaxy-QSO). Out of the 175,545 fitting results we assigned priority based on the following criteria:

i- The fit significantly improves by adding a set of components at a second redshift, i.e. it corresponds to large χ^2 difference. The threshold was set based on the values extracted for the four known candidates and by visual inspection of the fitting results for various χ^2 difference values.

ii- The peaks of the χ^2 difference do not correspond to fits with unphysical properties (e.g. negative emission lines). Negative residuals are common when fitting the spectra with one set of components. Their strength, and therefore their impact in the results, can vary from very weak features usually caused by details in the continuum fitting and the presence of noise, to very strong features caused by poor fitting of emission lines. To exclude the latter cases (but not the former) from our final sample we examine only peaks of the χ^2 differences that correspond to positive differences between the 99.5% and the 0.5% quartiles of the distribution of fluxes per pixel in each fitted spectrum (for each set of components).

iii- The peaks of the χ^2 difference correspond to a difference in redshift between the two sources larger than 0.01.

In the case that Galaxy-QSO fitting was performed to the spectra, there was a lot of contamination to our results due to two additional reasons:

i- In most of the cases the fitting of the narrow emission lines at the SDSS redshift by the galaxy components was resulting to unusual residuals of the broad lines, (e.g. in the case that no significant shift was present between the NLs and BLs), which were then fitted very poorly by the second set of components. To exclude these objects from our final sample we also measured the χ^2 value of the fit by the second set of components restricted to an area of 500 Å around the Hα line and 200 Å around the Hβ line. Peaks corresponding to a very large value of χ^2 at the areas of the BLs were excluded.

ii- In all cases the fitting of a QSO spectrum by the galaxy components will improve significantly when the QSO components are added to the fit. That is due to the fit of the broad emission lines by the second set of components. To make sure that the observed improvements were not only caused by this, we re-perform the fitting of the spectrum by two sets of QSO components, at the redshifts suggested by the Galaxy-QSO fitting.

The fits of the spectra selected using the above criteria were visually inspected independently by two of the authors (PT and RD). The fitting results showed that there is a lot of contamination, e.g. from obvious Double Peaked Emitters (DPEs), misclassified objects in SDSS or spectra with wrong estimated redshifts. By excluding all those cases, the most interesting objects were identified. In Figure 1 we provide an example of the fitting output for one of those sources.

The objects selected here are presented in detail in the following section. We should point out that all the objects selected for their interesting features are at redshifts below 0.8. For higher redshifts the [O III] line is not included in the spectra and the differences in the fitting are detected mainly based on the [O II] line, which in most of the cases is very faint or not well detected. For this reason no reliable information for the narrow emission lines are included in most of the spectra at higher redshifts.

TABLE 1
Summary of the peculiar objects found with our code. (1) Quasar name. (2-3) Right ascension and declination (J2000.). (4) Modified Julian Date of the SDSS observation. (5) Plate. (6) Fiber. (7) Redshift of Narrow Lines. (8) Redshift of broad lines. (9) Method used to select the target. QG: Quasar–Galaxy; QQ - Quasar–Quasar; GQ: Galaxy–Quasar (see the text for the method description). (10) Classification: A- Asymmetric BL profile; B- Black hole binary candidate; D- Double-peaked emitter; E- Extreme double-peaked emitter; O- Others (see section 3).

Obj.name (1)	R.A. (2)	Dec. (3)	MJD (4)	Plate (5)	Fiber (6)	$z_{\rm NL}$ (7)	$z_{\rm BL}$ (8)	Method (9)	Class. (10)
J0012-1022	00:12:24.03	-10:22:26.3	52141	0651	072	0.228	0.221	QG,QQ	A
J0155-0857	01:55:30.02	-08:57:04.0	52168	0665	597	0.165	0.170	QQ	O
J0221+0101	02:21:13.15	+01:01:02.9	51869	0406	374	0.354	0.364	QG,QQ	O
J0829+2728	08:29:30.60	+27:28:22.7	52932	1267	066	0.321	0.325	GQ	O
J0918+3156	09:18:33.82	+31:56:21.2	52990	1592	139	0.452	0.457	QQ,GQ	D
J0919+1108	09:19:30.32	+11:08:54.0	53050	1740	399	0.369	0.372	QQ	O
J0921+3835	09:21:16.13	+38:35:37.6	52731	1214	293	0.187	0.182	QQ	A
J0927+2943	09:27:12.65	+29:43:44.1	53389	1939	467	0.713	0.698	QG,QQ	B
J0931+3204	09:31:39.05	+32:04:00.2	53386	1941	553	0.226	0.226	QQ,GQ	O
J0932+0318	09:32:01.60	+03:18:58.7	52254	0568	039	0.420	0.401	QQ	B,D
J0936+5331	09:36:53.85	+53:31:26.9	52281	0768	473	0.228	0.237	QQ	A
J0942+0900	09:42:15.12	+09:00:15.8	52757	1305	281	0.213	0.168	GQ	E
J0946+0139	09:46:03.95	+01:39:23.7	51989	0480	480	0.220	0.227	QQ	A
J1000+2233	10:00:21.80	+22:33:18.6	53737	2298	102	0.419	0.377	GQ	E,B
J1010+3725	10:10:34.28	+37:25:14.8	52993	1426	110	0.282	0.276	QG,QQ	O
J1012+2613	10:12:26.86	+26:13:27.3	53757	2347	513	0.378	0.351	QQ	E,B
J1027+6050	10:27:38.54	+60:50:16.5	52375	0772	216	0.332	0.301	QQ	E
J1050+3456	10:50:41.36	+34:56:31.4	53431	2025	603	0.272	0.258	QQ,GQ	B
J1105+0414	11:05:39.64	+04:14:48.2	52356	0581	226	0.436	0.406	GQ	E
J1117+6741	11:17:13.91	+67:41:22.7	51942	0491	402	0.248	0.253	GQ	O
J1154+0134	11:54:49.42	+01:34:43.6	52051	0515	099	0.469	0.450	QQ	A,B
J1207+0604	12:07:55.83	+06:04:02.8	52376	0842	530	0.136	0.128	GQ	O
J1211+4647	12:11:13.97	+46:47:12.0	53116	1449	001	0.294	0.287	QQ,GQ	O
J1215+4146	12:15:22.78	+41:46:21.0	53120	1450	141	0.196	0.206	QQ,GQ	O
J1216+4159	12:16:09.60	+41:59:28.4	53120	1450	130	0.242	0.233	GQ	O
J1328-0129	13:28:34.15	-01:29:17.6	52426	0911	333	0.151	0.140	QQ,GQ	O
J1414+1658	14:14:42.03	+16:58:07.2	54523	2758	014	0.237	0.242	QQ	O
J1440+3319	14:40:05.31	+33:19:44.5	53498	1646	283	0.179	0.165	GQ	D
J1536+0441	15:36:36.22	+04:41:27.0	54567	1836	270	0.389	0.373	QG,QQ	D,B
J1539+3333	15:39:08.09	+33:33:28.0	52823	1355	572	0.226	0.199	QG,QQ	O,B
J1652+3123	16:52:55.90	+31:23:43.8	52790	1343	593	0.593	0.590	QG,QQ,GQ	O
J1714+3327	17:14:48.51	+33:27:38.3	54591	2973	190	0.181	0.186	QQ	O,B

3. RESULTS

Our selection produced a list of 32 candidates of particular relevance (see Table 1). For each target, we reanalyzed the SDSS spectrum, modeling it with a power law for the QSO continuum emission, a host galaxy template at the redshift of the NLs and a template of the iron complex, as described in Decarli et al. (2010a) and De Rosa et al. (2011). We fitted the broad components of Mg II, Hβ and Hα with 2 gaussian functions at the same peak. This fitting approach aims to better constrain the peak wavelength, and is not meant to reproduce the line profile in detail. Narrow lines are masked when fitting the broad component; by construction of our sample, there is a velocity offset between BLs and NLs. This simplifies the measurement of the peak wavelengths of the two components.

Peak wavelengths are then converted into velocity shifts:

$$v_{\rm BL} = c\frac{z_{\rm BL} - z_{\rm NL}}{1 + z_{\rm NL}}. \quad (2)$$

Continuum-subtracted velocity plots of all the interesting targets are shown in Figure 2.

A rough classification scheme was set according to: 1) the magnitude of the velocity shift, in particular when comparing Mg II and Balmer lines; 2) the presence of strong asymmetries in the line profiles; 3) the occurrence of secondary bumps or peaks; 4) additional information from other emission lines or from the SDSS images. We define five classes of objects, namely; *i*) **black hole binary candidates**, which are expected to show similar velocity shifts for all the BLs, and a variety of line profiles (e.g., Shen & Loeb 2010). *ii*) quasars with **asymmetric line profiles**, with small ($\lesssim 2\,000$ km s^{-1}) shifts of BL peaks. These features are observed in some "normal" type-I AGN, and they are possibly related to asymmetries in the BL region (e.g., Bentz et al. 2010). They may also be associated to a velocity-dependent Balmer decrement of broad lines. *iii*) **double peaked emitters** (DPEs), characterized by symmetric features in line profiles (e.g., a secondary peak in the red wing of the line, at the opposite velocity with respect to a blue-shifted peak). Another property of DPEs is that different lines (in particular low- and high-ionization lines) may show very different shapes and shifts (Halpern et al. 1996). These properties are usually associated to a disk-like structure

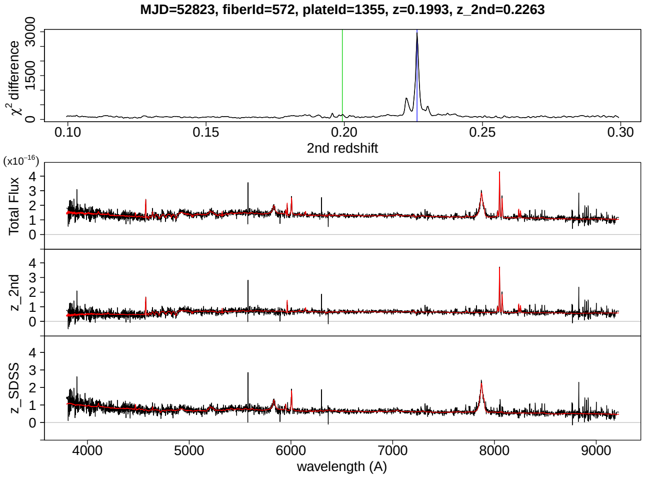

FIG. 1.— An example of an interesting object (J1539+3333) detected by the method. **Top panel:** The χ^2 difference between the fitting of the spectrum with 1 and 2 sets of components at different redshifts. The green and blue lines represent the SDSS redshift ($z_{\rm sdss}$) and the one with the largest χ^2 difference ($z_{\rm fit}$). **2nd panel:** The fitting of the spectrum (black) with both sets of components (red). **3rd panel:** Black line: residuals after subtracting the fit components $z_{\rm sdss}$. The fit with the set of components at $z_{\rm fit}$ is shown in red. **Bottom panel:** Black line: residuals after subtracting the fit at $z_{\rm fit}$. Red line: the fit with the set of components at $z_{\rm sdss}$. A color version of the plot is available in the electronic version of the paper.

of the BL region (Eracleous & Halpern 1994). *iv*) **extreme double peaked emitters** (see below). *v*) **others**, i.e. objects with small shifts or poor signal-to-noise spectra, preventing us from a clear interpretation, or objects with very peculiar properties, not belonging to any of the aforementioned classes.

Note that all the BHB candidates with small velocity shifts could also be recoiling BHs, though they are expected to be rarer than binaries (Dotti et al. 2009; Volonteri et al. 2010)[6]. In the following, we will not distinguish between these two cases, including both in the "BHB candidates" class.

This classification produced 9 BHB candidates, including the 5 known candidates. For the new 4 sources, other interpretations are also plausible, including an extremely rare case of quasar–galaxy superposition for one of them. Five quasars show very high velocity shifts ($\gtrsim 5\,000$ km s^{-1}) and relatively faint lines. These objects probably represent extreme cases of DPEs (hereafter, they will be referred to as EDPEs). In the following, we discuss the properties of each source individually, reporting our interpretation on the nature of the object.

J0012-1022

The Balmer broad lines of this $z_{\rm NL} = 0.228$ quasar show a peak $\sim 1\,700$ km s^{-1} blue-shifted with respect to narrow lines. The line profile is clearly asymmetric. Hα and Hβ have identical profiles, with $F({\rm H}\alpha) = 2.6F({\rm H}\beta)$. A bump in the red wing of Balmer lines suggests that this is a strongly asymmetric double-peaked emitter (see also Strateva et al. 2003; Shen et al. 2010), though Shen & Loeb (2010) showed that the line profile of this source can be ascribed to an unequal mass BHB. **Classified: asymmetric line profile.**

J0155-0857

The Hα line of this source shows a small ($\sim 1\,500$ km s^{-1}) red-shift with respect to the narrow lines. A slight asymmetry in the line profile is reported. The asymmetry is clearer in the Hβ profile, which peaks at longer wavelengths ($\Delta v \approx 2\,200$ km s^{-1}). Shen et al. (2010) reported a blue-shift of ~ 600 km s^{-1} for Hα and $\sim 2\,300$ km s^{-1} for Hβ. The relatively small velocity shift and the difference in the profiles of Balmer lines suggest that this is a normal quasar. **Classified: others.**

J0221+0101

Both Hα and Hβ broad components of this $z_{\rm NL} = 0.354$ quasar show a $\sim 1\,300$ km s^{-1} shift with respect to the narrow lines. Line profiles are rather boxy with no obvious asymmetry. Shen et al. (2010) report no significant shift for Hα, and an exceedingly pronounced shift for Hβ ($\sim 3\,100$ km s^{-1}). **Classified: others.**

J0827+2728

The Balmer lines of this quasar show a small (~ 900 km s^{-1}) red-shift with respect to the NLs, which may also be consistent with a strongly asymmetric line profile. **Classified: others.**

J0918+3156

The peculiar properties of this object were first reported by Bonning, Shields & Salviander (2007). The Mg II and Hβ broad lines are red-shifted with respect to the NLs. However, the shift is $\sim 3\,000$ km s^{-1} for Hβ and only ~ 1050 km s^{-1} for Mg II (see Bonning, Shields & Salviander 2007; Shen et al. 2010), suggesting that the shift is due neither to a BHB nor a recoil. **Classified: double peaked emitter.**

J0919+1108

The broad emission lines of this source are slightly red-shifted ($700 - 1\,000$ km s^{-1}, depending on the subtraction of the [N II] lines). The SDSS image of the quasar reveals a complex morphology, probably resulting by a strong gravitational interaction or a merger with a nearby galaxy. Shen et al. (2010) reported a blue-shift for the broad component of Hα and a red-shift for Hβ, which is not confirmed in our analysis. **Classified: others.**

J0921+3835

This object shows clearly asymmetric Balmer lines, with a peak at $\sim 1\,200$ km s^{-1} blue-wards (consistent with the values reported by Shen et al. 2010). The Hα/Hβ flux ratio is ~ 3.3. An unidentified line is observed at 5812 Å, corresponding to a $\sim 2\,300$ km s^{-1} shift with respect to the Hβ rest frame. A similar peak is not observed in the Hα profile. **Classified: asymmetric line profile.**

---

[6] Note that these estimates could be affected by our incomplete understanding of the orbital decay of binaries at subparsec scales (see, e.g. Colpi & Dotti 2009; Lodato et al. 2009).

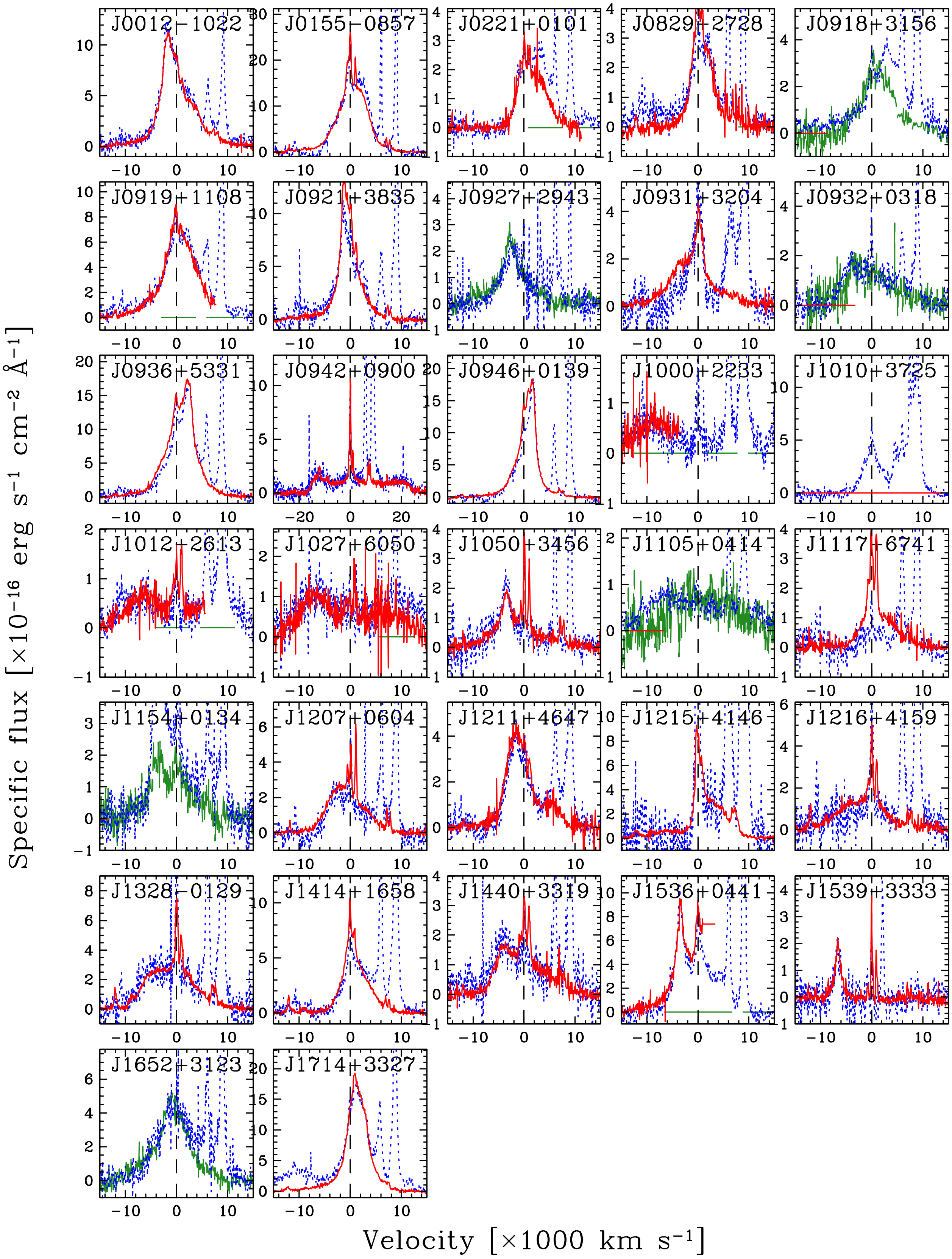

FIG. 2.— Velocity diagrams of Hα (red, solid lines), Hβ (blue, dotted lines) and Mg II (green, dashed lines) for all our candidates. The flux of Hβ is scaled up to match the one of Hα or Mg II.

J0927+2943

One of the known BHB candidates (Bogdanovic, Eracleous & Sigurdsson 2009; Dotti et al. 2009). This quasar was first reported by Komossa, Zhou & Lu (2008) as a recoiling BH candidate. Three sets of lines are observed, two narrow systems at $z = 0.713$ and $z = 0.699$ and a broad line system consistent with the second set of narrow lines. The shift between the two redshifts is $\sim 2\,600$ km s^{-1}. This object has been interpreted as a chance superposition in a galaxy cluster by Heckman et al. (2009) and Shields, Bonning & Salviander (2009). However, later observational follow-ups have disproved the presence of a galaxy cluster in the source field (Decarli, Reynolds & Dotti 2009). **Classified: black hole binary candidate.**

J0931+3204

The spectrum of this quasar shows relatively broad and asymmetric narrow lines, which makes the determination of $z_{\rm NL}$ uncertain. The blue wing of Hα shows a bump at $\sim 3\,500$ km s^{-1} with respect to the peak of the line. This feature is not observed in Hβ. This object was not reported in previous studies of quasars with peculiar NL profiles (e.g. Wang et al. 2009; Liu et al. 2010a,b). Shen et al. (2010) flagged this source as a DPE candidate. **Classified: others.**

J0932+0318

This source shows a shift of $\sim 4\,000$ km s^{-1} in the peak of the Mg II and the Hβ lines. Shen et al. (2010) reported two different velocity offsets for Hβ ($\sim 3\,900$ km s^{-1}) and Mg II ($\sim 1\,100$ km s^{-1}) respectively, but such a difference is not confirmed by our analysis. The Hβ line appears slightly asymmetric, though the line profile is poorly determined. This object has been studied in detail by Barrows et al. (2011), who suggested it to be a DPE from an asymmetric BL region, or a BHB. **Classified: double peaked emitter** or **black hole binary candidate.**

J0936+5331

The Balmer lines of this $z_{\rm NL} = 0.228$ quasar show a strongly asymmetric profile, with a bright blue peak at $2\,100$ km s^{-1} (2250 km s^{-1} in the analysis by Shen et al. 2010) with respect to the narrow lines. The red wing of Hα is 3.1× brighter than Hβ; the blue wing is 4.0× brighter. No peak or bump is observed in the blue wing at $2\,100$ km s^{-1}. This source was listed in the "DPE Auxiliary sample" by Strateva et al. (2003). **Classified: asymmetric line profile.**

J0942+0900

This object has been labeled as a galaxy by the SDSS automatic pipeline, presumably because the broad lines are too flat and extended. The Balmer lines are $\sim 38\,000$ km s^{-1} broad (the broadest ever reported!) and asymmetric (the blue peak is brighter and peaks around $\sim -11\,500$ km s^{-1}, while the red side is fainter, flatter and extends red-wards of $+20\,000$ km s^{-1}). The flux ratio between Hα and Hβ is 2.6, and the lines have similar profile. This object is the most extreme DPE ever discovered in terms of line width. This object may also represent the prototypal to explain the peculiar features of other (less extreme and fainter) cases (e.g., J1000+2233, J1012+2613, etc). **Classified: extreme double peaked emitter.**

J0946+0139

The Balmer lines of this $z_{\rm NL} = 0.2203$ quasar peak at 1550 km s^{-1} blue-wards of the NL system (see also Shen et al. 2010). Boroson & Lauer (2010) reported an "anomalous Hβ profile" for this source. The broad lines show no obvious second peak, but the blue wings are slightly more extended than the red ones. Also, the flux ratio between Hα and Hβ is larger in the blue wing. **Classified: asymmetric line profile.**

J1000+2233

This source was serendipitously discovered by our group (Decarli et al. 2010b) out of the SDSS database, and share some of the properties of J0942+0900. The Balmer lines appear faint and extremely blue-shifted ($\sim 8\,700$ km s^{-1}). Also the Mg II line shows a blue-shift, but its magnitude is poorly constrained since the line is only partially covered by the SDSS spectrum. This quasar was labeled as a galaxy by the SDSS pipeline. Shen et al. (2010) reported inconsistent velocity offsets for Hβ ($4\,500$ km s^{-1} *red*-wards) and Mg II ($2\,700$ km s^{-1} blue-wards). **Classified: extreme double peaked emitter** or **black hole binary candidate.**

J1010+3725

This object shows a complex [O III] profile (both for the 4959 and the 5 008 Å emission lines). Two peaks are observed, with a velocity difference of $\sim 1\,400$ km s^{-1}. The blue peaks are fainter. Other narrow emission lines (Hβ, Hα, [S II]) appear normal. This source was labeled as "anomalous [O III] profile" by Boroson & Lauer (2010). A peculiar [O III] profile was also reported by Shen et al. (2010). This quasar was not included in previous studies on double-peaked NL objects (e.g. Wang et al. 2009; Liu et al. 2010a,b). **Classified: others.**

J1012+2613

The Balmer lines of this $z_{\rm NL} = 0.3783$ quasar show similar properties to those of J1000+2233: The BLs peak $\sim 6\,000$ km s^{-1} blue-wards of the NLs. The red wing of Hα and the blue wing of Mg II are not covered. **Classified: extreme double peaked emitter** or **black hole binary candidate.**

J1027+6050

This is the only EDPE already known (Strateva et al. 2003). The blue peaks of Hα and Hβ are $7\,000$ km s^{-1} blue-shifted with respect to NLs. The shift is missed in the analysis by Shen et al. (2010), probably because of the faintness of the lines. **Classified: extreme double peaked emitter.**

J1050+3456

This source was discovered by Shields et al. (2009) out of the SDSS database. The broad component of Balmer lines is clearly shifted ($\sim 3\,400$ km s^{-1} blue-wards; a similar value was found by Shen et al. 2010). No NL is observed at the redshift of the BLs. **Classified: black hole binary candidate.**

J1105+0414

This quasar was found in the galaxy sample. The broad Hβ line peaks $\sim 6\,000$ km s^{-1} blue-wards of the narrow component. Due to its faintness, the line profile is poorly constrained. The Mg II line is equally faint, but no obvious shift is observed, supporting the DPE interpretation for this source. **Classified: extreme double peaked emitter.**

J1117+6741

The Hα broad component of this source appears slightly redshifted with respect to the NLs. The properties of Hβ are difficult to characterize, due to its intrinsic faintness. **Classified: others.**

J1154+0134

The Hβ and Mg II lines of this $z_{\rm NL} = 0.469$ quasar have identical profiles, with a peak $\sim 3\,500$ km s^{-1} blue-wards of the expected wavelengths and a rather broad red wing. The line profiles resemble the one of other sources with asymmetric lines (e.g., J0012-1022), but the magnitude of the shift and the similarity between Hβ and Mg II support the BHB hypothesis. The low S/N of the spectrum of the SDSS spectrum hinder any conclusion on the nature of this source. **Classified: asymmetric line profile** or **black hole binary candidate.**

J1207+0604

The broad component of the Balmer lines of this quasar is rather symmetric but shifted $\sim 2\,500$ km s^{-1} blue-wards with respect to NLs. The flux ratio between Hα and Hβ is ~ 4, roughly constant with respect to the line-of-sight velocity. This source was not included in the compilation by Shen et al. (2010). **Classified: others.**

J1211+4647

The bulk of the Balmer line broad components of this source is shifted $\sim 1\,700$ km s^{-1} blue-wards of the NL system (consistent values are reported in Shen et al. 2010). The Hα/Hβ flux ratio is ~ 4, constant along the velocity profile. The Hα line shows a bump at $\sim 6\,000$ km s^{-1} in the red wing, possibly revealing the DPE-like nature of this source. Such a feature is not clearly observed for Hβ because of the superposition of the [O III] doublet. **Classified: others.**

J1215+4146

This quasar shows a peculiar Balmer line profile. The bulk of Hα emission arises from a bright bump in the red wing. The blue side of the line may also present a faint wing, the actual presence of which depends on the continuum modeling. At zero order, the Hβ line shows analogous profile. However, the feature in the red wing is ~ 11 times fainter than what observed in Hα. The interpretation of this object is unclear. Boroson & Lauer (2010) labeled this source as a 'no broad line' quasar. **Classified: others.**

J1216+4159

The Hα broad emission of this quasar is clearly blue-shifted ($\sim 2\,300$ km s^{-1}). The line profile shows no relevant asymmetry. The Hβ broad component is barely detected, its flux being ~ 7 times fainter than Hα. **Classified: others.**

J1328-0129

The broad component of the Balmer lines in this $z_{\rm NL} = 0.1514$ quasar are blue-shifted ($\sim 3\,100$ km s^{-1}) with respect to NLs. The line profile is boxy, with no significant asymmetry. The Hα/Hβ flux ratio is ~ 5, constant over the velocity range. This object was not included in the analysis by Shen et al. (2010). Strateva et al. (2003) and Bian et al. (2007) listed this source as a DPE. **Classified: others.**

J1414+1658

The bulk of the BLs of this quasars is redshifted ($\sim 1\,200$ km s^{-1}) with respect to NLs. The red wing is brighter. The Hα/Hβ flux ratio is ~ 4 in the blue wing and around 3 in the red wing. This object was labeled as a DPE candidate by Shen et al. (2010). **Classified: others.**

J1440+3319

The Hα line of this source peaks at $\sim 3\,700$ km s^{-1} blue-wards of the NLs, and shows an extended red wing. The Hβ line profile is similar. The properties of this quasar are half the way between the objects with asymmetric line profiles (e.g., J1154+0134) and the typical DPEs, though this source has not been included in any previous compilation of DPEs. **Classified: double peaked emitter.**

J1536+0441

The peculiar properties of this object were first reported by Boroson & Lauer (2009). The broad lines show two peaks, one consistent with the rest-frame of the galaxy as set by NLs, the other significantly blue-shifted ($\sim 3\,400$ km s^{-1}). Boroson & Lauer (2009) proposed the BHB interpretation for this source. However, following observations covering the red wing of Hα revealed the presence of a bump in the line wing (Chornock et al. 2010), a feature commonly observed in DPEs. **Classified: double peaked emitter** or **black hole binary candidate.**

J1539+3333

From the spectroscopic point of view, the properties of this source are similar to those of J0927+2943. The spectrum presents three sets of lines at two different redshifts:

Broad balmer lines (driving the redshift estimate by the SDSS pipeline) and faint narrow lines are detected at $z_1 = 0.1993$. Another set of (brighter) narrow lines is observed at $z_2 = 0.2263$. The corresponding velocity shift is $\sim 6\,600$ km s^{-1}. A careful inspection of the SDSS image of this source reveals an extended stellar wing Southwards of the quasar. If this belongs to the quasar host galaxy, then it would reveal a strongly perturbed morphology. On the other hand, it could be that this is a superposed galaxy. In this case, since $z_{\rm BL} < z_2$, the galaxy would be in the background of the quasar. This scenario is usually extremely unlikely, given the high velocity differences (Dotti & Ruszkowski 2010). However, the SDSS image reveals the presence of a rich galaxy cluster South-West of the quasar, which may enhance the galaxy density on the sky plain by few orders of magnitudes. Follow-up observations aimed at directly measuring the redshift of the stellar wing are needed to fully understand the nature of this source. **Classified: black hole binary candidate** or **others**.

J1652+3123

The Hβ and Mg II broad lines of this $z_{\rm NL} = 0.5929$ quasar show a small blue-shift (~ 500 km s^{-1}) with respect to NLs. The line profiles are similar and do not show any significant asymmetry. Our shift estimates are consistent with those reported by Shen et al. (2010). Given the small velocity difference, this source is probably a normal quasar (Bonning, Shields & Salviander 2007). **Classified: others.**

J1714+3327

The Balmer lines of this source show a clear red-shift ($\sim 1\,300$ km s^{-1}, consistent with the values reported in Shen et al. 2010). The line profiles are symmetric. The Hα/Hβ flux ratio is around 3. **Classified: others** or **black hole binary candidate.**

4. SUMMARY & DISCUSSION

We presented the outcome of our automatic and systematic search for massive BHBs. We have found 9 BHB candidates in the SDSS DR7. Of these, 5 have already been extensively discussed in literature. The 4 new candidates are J1012+2613, J1154+0134, J1539+3333 and J1714+3327. For each one of them a BHB is not the only possible explanation: The peculiar spectrum of J1012+2613 can be explained also as an extreme case of double peaked emitter; J1154+0134 has a too noisy spectrum to exclude other explanations; J1539+3333 may be a rare superposition of a quasar and a galaxy; The small shift between broad and narrow lines in J1714+332 ($\approx 1\,300$ km s^{-1}) does not necessarily imply the presence of a BHB. A more detailed understanding of the expected spectral features of BHBs and observational follow-ups are needed to confirm or dismiss the BHB hypothesis for all the 9 candidates presented here.

Our method also automatically detected a number of other interesting objects with peculiar spectral features:

i- 4 objects show strong asymmetries in the line profiles, with a peak offset $\gtrsim 2\,000$ km s^{-1} (either red- or blue-wards) and a longer wing in the opposite velocity range with no secondary peak.

ii- 3 objects have BL properties analogous to what typically observed in DPEs, even if the secondary peak is not prominent. None of them appeared in the compilation by Strateva et al. (2003).

iii- We provide strong evidence of a new class of extreme double-peaked emitters, with very broad (FWHM>10 000 km s^{-1}) and rather faint emission lines. The main peak of these lines show huge velocity shifts ($> 5\,000$ km s^{-1}) with respect to the NLs. For a comparison, only 5 objects out of 138 in Strateva et al. (2003) have a shift of the brighter peak of Hα larger than 5 000 km s^{-1}, and none of them exceed 7 000 km s^{-1}. Note that the "extreme double-peaked emitter" explanation is possible also for one of the BHB candidates already discussed in literature (J1000+2233, Decarli et al. 2010b).

iv- out of the remaining 13 quasars, 12 show clear yet relatively small (500–3 000 km s^{-1}) velocity offsets between NLs and BLs, and no obvious asymmetries in the line profiles of the broad components.

v- the case of J1539+3333 is worth of specific discussion. This quasar has few spectral features in common with the BHB candidate J0927+2943, with a set of broad and narrow emission lines shifted with respect to a brighter set of narrow emission lines. However, the velocity shift is extremely high ($\approx 6\,600$ km s^{-1}). As a consequence, this object cannot be explained in terms of a recoiling BH, since the maximum kick velocity has been constrained with fully GR simulations to be $\lesssim 4\,000$ km s^{-1}(Baker et al. 2007; Herrmann et al. 2007; Campanelli et al. 2007; Schnittman & Buonanno 2007; Lousto & Zlochower 2009; van Meter et al. 2010). A natural explanation can be a superposition of an AGN and a galaxy within a galaxy cluster. Such model has been ruled out for J0927+2943 because no galaxy cluster was observable in the field (Decarli, Reynolds & Dotti 2009). For J1539+3333 a superposition is not ruled out by observations. The redshift of this source is $z \approx 0.2$, close to the theoretically estimated peak of superpositions in clusters (Dotti & Ruszkowski 2010). However, the line shift corresponds to a relative velocity between the two galaxies $\gtrsim 1.5$ times larger than the maximum relative velocity theoretically expected (Dotti & Ruszkowski 2010). A better comprehension of this peculiar object needs a more detailed study of its field, as already performed for J0927+2943 (Decarli, Reynolds & Dotti 2009) and J1536+0441 (Decarli et al. 2009; Wrobel & Laor 2009).

ACKNOWLEDGMENTS

The authors would like to thank C. A. L. Bailer-Jones and F. Walter for useful discussions and support. DWH was partially supported by the NSF (grant AST-0908357) and a research fellowship from the Alexander von Humboldt Foundation.

Funding for the Sloan Digital Sky Survey (SDSS) has been provided by the Alfred P. Sloan Foundation, the Participating Institutions, the National Aeronautics and Space Administration, the National Science Foundation, the U.S. Department of Energy, the Japanese Monbukagakusho, and the Max Planck Society. The SDSS Web site is http://www.sdss.org/. The SDSS is managed by the Astrophysical Research Consortium (ARC) for the Participating Institutions. The Participating Institutions are The University of Chicago, Fermilab, the Institute for Advanced Study, the Japan Participation Group, The Johns Hopkins University, the Korean Scientist Group, Los Alamos National Laboratory, the Max-Planck-Institute for Astronomy (MPIA), the Max-Planck-Institute for Astrophysics (MPA), New Mexico State University, University of Pittsburgh, University of Portsmouth, Princeton University, the United States Naval Observatory, and the University of Washington.

REFERENCES

Baker J.G., Boggs W.D., Centrella J., Kelly B.J., McWilliams S.T., Miller M.C., van Meter J.R., 2008, ApJ Letter, 682, 29

Barrows R.S., Lacy C.H.S., Kennefick D., Kennefick J., Seigar M.S., 2011, NewA, 16, 122

Begelman M.C., Blandford R.D., Rees M.J., 1980, Nature, 287, 307

Bentz M.C., Walsh J.L., Barth A.J., Yoshii Y., Woo J.-H., Wang X., Treu T., Thornton C.E., et al., 2010, ApJ, 716, 993

Bian W.-H., Chen Y.-M., Gu Q.-S., Wang J.-M., 2007, ApJ, 668, 721

Bogdanovic T., Reynolds C.S., Miller M.C., 2007, ApJ Letter, 661, 147

Bogdanovic T., Smith B.D., Sigurdsson S., Eracleous M., 2008, ApJS, 174, 455

Bogdanovic T., Eracleous M., Sigurdsson S., 2009, ApJ, 697, 288

Bogdanovic T., Eracleous M., Sigurdsson S., 2009b, New Astronomy Review, 53, 113

Bonning E.W., Shields G.A., Salviander S., 2007, ApJ Letters, 666, 13

Boroson T.A., Lauer T.R., 2009, Nature, 458, 53

Boroson T.A., Lauer T.R., 2010, AJ, 140, 390

Campanelli M., Lousto C.O., Zlochower Y., Merritt D. 2007, ApJ Letter, 659, 5

Chornock R., Bloom J.S., Cenko S.B., Filippenko A.V., Silverman J.M., Hicks M.D., Lawrence K.J., Mendez A.J., et al., 2010, ApJ Letters, 709, 39

Colpi M, Dotti M., 2009, ASL in press (arXiv0906.4339)

Decarli R., Dotti M., Falomo R., Treves A., Colpi M., Kotilainen J.K., Montuori C., Uslenghi M., 2009, ApJ Letters, 703, 76

Decarli R., Reynolds M., Dotti M., 2009, MNRAS, 397, 458

Decarli R., Falomo R., Treves A., Kotilainen J.K., Labita M., Scarpa R., 2010a, MNRAS, 402, 2441

Decarli R., Dotti M., Montuori C., Liimets T., Ederoclite A., 2010b, ApJ Letters, 720, 93

De Rosa G., Decarli R., Walter F., Fan X., Jiang L., Kurk J., Pasquali A., Rix, H.W., 2011, ApJ, in press

Dotti M., Montuori C., Decarli R., Volonteri M., Colpi M., Haardt F., 2009, MNRAS Letters, 398, 73

Dotti M., Ruszkowski M., 2010, ApJ Letter, 713, 37

Dotti M., Volonteri M., Perego A., Colpi M., Ruszkowski M., Haardt F., 2010, MNRAS, 402, 682

Eracleous M., Halpern J.P., 1994, ApJS, 90, 1

Halpern J.P., Eracleous M., Filippenko A.V., Chen K., 1996, ApJ, 464, 704

Heckman T.M., Krolik J.H., Moran S.M., Schnittman J., Gezari S., 2009, ApJ, 695, 363

Herrmann F., Hinder I., Shoemaker D.M., Laguna P., Matzner R. A., 2007, Phys. Rev. D, 76, 084032

Kesden M., Sperhake U., Berti E., 2010, ApJ, 715, 1006

Komossa S., Burwitz V., Hasinger G., Predehl P., Kaastra J.S., Ikebe Y., 2003, ApJ Letters, 582, 15

Komossa S., Zhou H., Lu H., 2008, ApJ Letters, 678, 81

Liu X., Shen Y., Strauss M.A., Greene J.E., 2010a, ApJ, 708, 427

Liu X., Greene J.E., Shen Y., Strauss M.A., 2010b, ApJ Letters, 715, 30

Lodato G., Nayakshin S., King A.R., Pringle J.E., 2009, MNRAS Letters, 398, 1392

Lousto C.O., Zlochower Y. 2009, Phys. Rev. D, 79, 064018

Maness H.L., Taylor G.B., Zavala R.T., Peck A.B., Pollack L.K., 2004, ApJ, 602, 123

Montuori C., Dotti M., Colpi M., Decarli R., Haardt F., 2010, MNRAS in press (arXiv:1010.4303)

Popovic L.C., Shapovalova A.I., Ilic D., Kovacecic A., Kollatschny W., Burenkov A.N., Chavushyan V.H., Bochkarev N.G., Leon-Tavares J., 2011, A&A, in press (arXiv:1101.4867)

Rodriguez C., Taylor G.B., Zavala R.T., Pihlstrom Y.M., Peck A.B., ApJ, 697, 37

Shields G.A., Bonning E.W., Salviander S., 2009, ApJ, 696, 1367

Schnittman J.D., Buonanno A., 2007, ApJ Letters, 662, 63

Shen Y., Hall P.B., Richards G.T., Schneider D.P., Strauss M.A., Snedden S., Bizyaev D., Brewington H., et al., 2010, submitted to ApJ (arXiv:1006.5178)

Shen Y., Loeb A., 2010, ApJ, 725, 249

Shields G.A., Rosario D.J., Smith K.L., Bonning E.W., Salviander S., Kalirai J.S., Strickler R., Ramirez-Ruiz E., Dutton A.A., Treu T., Marshall P.J., 2009, ApJ, 707, 936

Strateva I.V., Strauss M.A., Hao L., Schlegel D.J., Hall P.B., Gunn J.E., Li L.-X., Ivezić Ž., 2003, AJ, 126, 1720

Tsalmantza, P. & Hogg, D. W. 2011, submitted

Valtonen M.J., et al., 2008, Nature, 452, 851

van Meter J.R., Miller M.C., Baker J.G., Boggs W.D., Kelly B.J., 2010, ApJ, 719, 1427

Volonteri M., Miller J.M., Dotti M., 2009, ApJ Letters, 703, 86

Volonteri M., Gültekin K., Dotti M., 2010, MNRAS, 404, 2143

Wang J.-M., Chen Y.-M., Hu C., Mao W.-M., Zhang S., Bian W.-H., 2009, ApJ Letters, 705, 76

Wrobel J.M., Laor A., 2009, ApJ Letters, 699, 22